This journal is © The Royal Society of Chemistry 2023

Supporting information

High-performance heterostructure $Na_{0.7}MnO_{2.05}$-$Na_{0.91}MnO_2$ as lithium-free cathode for lithium-ion batteries

Tianfeng Gao,[a,b] Yanjun Cai,[a,b,*] Qingrong Kong,[a,b] Hualing Tian,[a,b] Xiang Yao,[a,b] Zhi Su[a,b,c,*]

Experimental section

Synthesis

The heterojunction cathode material $Na_{0.7}MnO_{2.05}$-$Na_{0.91}MnO_2$ was synthesized by solid-phase synthesis. The target material was prepared by solid-state method using CH_3COONa (Tianjin Zhiyuan) and $MnCO_3$ (aladdin) as raw materials with the molar ratio of Na: Mn=0.85:1 (20 mmol CH_3COONa:1.295 g, 20 mmol $MnCO_3$:2.300 g). The weighed chemical agents were mixed, and grind for 1 h in an agate mortar. The obtained precursors were calcined in a muffle furnace at 600 ℃ for 5 h, with a heating rate of 5 ℃ min^{-1}. Finally, the product was obtained with a yield of 84.13%. The sample was denoted as NMO600.

Material characterization

The crystal structures of the synthesized sample NMO600 was detected by X-ray diffraction (XRD, DX 2800). The morphology of the as-prepared material was characterized by field emission scanning electron microscopy (SEM, thermo scientific Apreo 2C), transmission electron microscopy (TEM, Talos F200S G2) and high-resolution transmission electron microscopy (HRTEM, Talos F200S G2)). X-ray energy dispersive spectrometry (EDS) was carried out to observe the distribution of each element in the material. The elemental composition and molecular structure were determined by Xray photoelectron spectroscopy (XPS, Al-Kα). The concentrations of Li^+ and Na^+ in electrolyte at the initial cycle were determined by inductively coupled plasma (ICP-OES/AES, Agilent 5110-ICP-OES).

Electrochemical measurements

In order to study the influence of loading mass on the performance of the battery, the loading amount of active material set as 0.5, 1.0, 1.5 and 2 mg cm^{-2}, respectively. The NMO600, acetylene black and polyvinylidene fluoride were mixed in a weight ratio of 8:1:1, and N-methylpyrrolidone was dropwise added and ground into slurry to prepare the working electrode. The slurry was uniformly spread onto the aluminum foil substrate and dried in a vacuum oven at 110 ℃ for 12 h. After cooling, the dried aluminum foil was cut into working electrodes (10 mm diameter disk). The coin battery was assembled in a vacuum glove box under the a high-purity argon atmosphere, and the water and oxygen contents were controlled to be less than 0.1 ppm. In the assembly process of the coin battery, the negative electrode shell, the lithium sheet, the diaphragm, the cathode electrode material, the gasket, the elastic sheet and the positive electrode shell are sequentially assembled, and about 90 μL of electrolyte is dropped in three times. The coin cell (2025) was assembled for lithium ion battery. The electrolyte was composed of ethylene carbonate (EC), dimethyl carbonate mixture (DMC), which dissolution of 1 mol L^{-1} $LiPF_6$ (the volume ratio of EC:DMC was 1:1). The Celgard 2400 microporous polyethylene film was chosen as the separator. Finally, the assembled lithium ion batteries were stationary for 12 h for electrochemical

performance test at 25 ℃. The electrochemical performance was tested using a battery test system (MIHW-200-160CH), the current density was 50 to 500 mA g^{-1} at 2-4.5 V (vs. Li/Li^+). Electrochemical impedance spectroscopy (EIS) was measured at a Zahner Elektrik electrochemical workstation (10^{-1} Hz to 10^5 Hz, 5 mV AC oscillation).

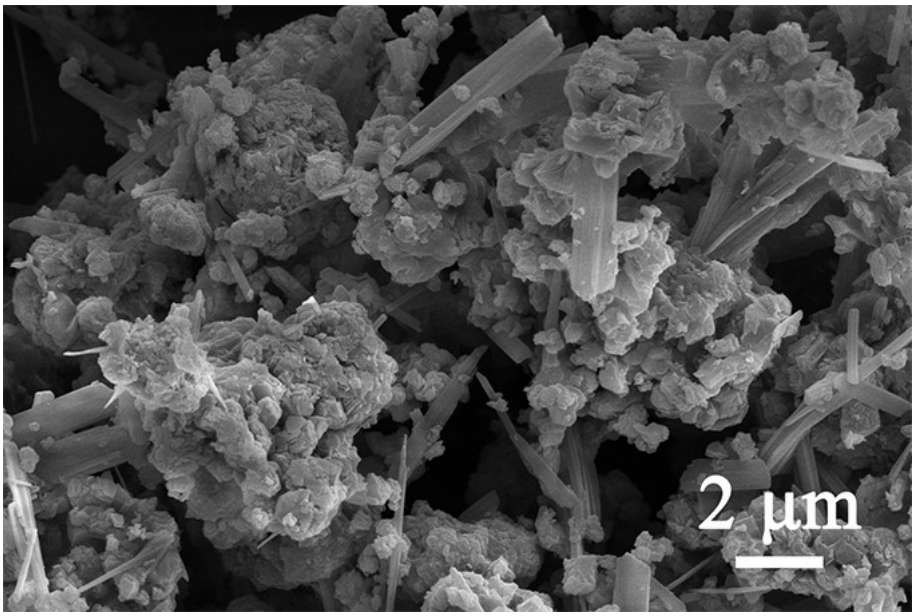

Fig. S1 The NMO600 of SEM image.

During the initial charging cycle, Na^+ ions were partially removed from the electrode material. Those Na^+ ions get into the electrolyte, which with a low concentration. The concentration of Na^+ ions at initial charging (constant 4.5 V) and discharging (2 V) was reduced from 30.24 mg L^{-1} to 24.09 mg L^{-1}, respectively, as shown in Table S1. This phenomenon indicated that trace Na^+ ions may be partially embedded back into NMO600. Those analysis results are consistent with reaction mechanism.

During charging at initial cycle, the partially Na^+ was removed from cathode $Na_{0.7}MnO_{2.05}$-$Na_{0.91}MnO_2$(Na_xMnO_2), the electrochemical reaction equation (1) as follows:

$$Na_xMnO_2 \longrightarrow yNa^+ + Na_xMnO_2 + ye^- \qquad (1)$$

In the anode, the Li^+ ions migrate to the negative electrode side to obtain electrons that transform into metallic the electrochemical reaction equation (2) as follows:

$$zLi^+ + ze^- \longrightarrow Li \qquad (2)$$

Table S1 The ICP-OES/AES test results.

sample	element	Weight (g)	Volume (mL)	Dilution factor	Instrument reading (mg/L)	concentration (mg/L)
initial charging (4.5 V)	Na	1	10	1	3.0242	30.2418
initial discharging (2 V)	Na	1	10	1	2.4087	24.0872
initial charging (4.5 V)	Li	1	25	1	5.5601	139.0017
initial discharging (2 V)	Li	1	25	1	4.3022	107.5544

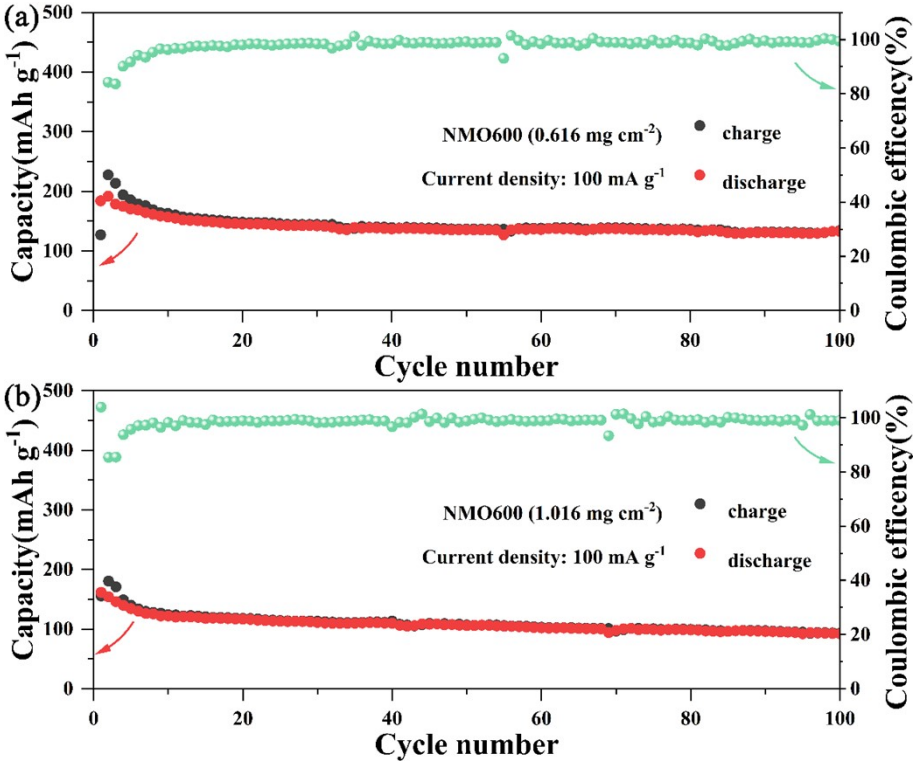

Fig. S2 Long cycle life of NMO600 (100 mA g^{-1}) for lithium ion batteries.

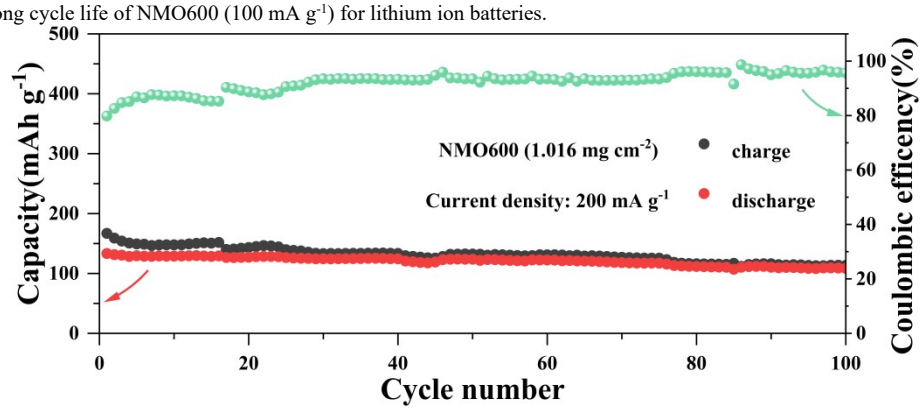

Fig. S3 Long cycle life of NMO600 (200 mA g^{-1}) for lithium ion batteries.

To understand the structural evolution of the NMO600 electrode in the charge-discharge process, ex situ XRD patterns between 2.0 V and 4.5 V were collected, as displayed in Fig. S4a. During the discharge process, the main diffraction peaks still belonged to the heterostructure. With Li^+ ions intercalation at the second discharging to 2 V, the $Na_{0.7-x}MnO_{2.05}$-$Na_{0.91-y}MnO_2$ and $Na_2Mn_5O_{10}$ was transformed to $Na_{0.7-x}Li_xMnO_{2.05}$-$Na_{0.91-y}Li_yMnO_2$. In addition, the main structure of NMO600 remains unchanged after 100 cycles at 1 A g^{-1}, which showing ultra-high structural reversibility. Fig. S4b shows the evolution of cell volume during the deintercalation and intercalation of Li^+. Compared with the electrode at 2.0 V, the cell volume of NMO600 only shrunk 2.27% and 5.04% when it was discharged

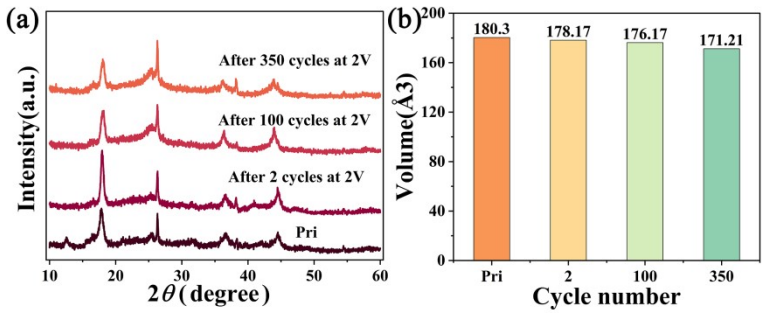

Fig. **S4** XRD patterns (a) and cell volume evolution (b) of NMO600 at selected states before cycling (pri), discharge to 2 V after 2nd ,100th and 350th cycles.

to 2.0 V after 100th and 350th cycles. The unique heterostructure contribute to alleviate structural strain. This is another reliable evidence for the structural stability of the layer-NMO600 electrode.[7]

Table S2 The manganese-based cathode materials for lithium-ion batteries.

Lithium free cathode	Current density (mA g^{-1})	Voltage range (V)	Initial capacity (mAh g^{-1})	Cycle number(n) /capacity (mAh g^{-1})	Ref.
$0.6Na_{0.7}MnO_2 \cdot 0.4Li_4Mn_5O_{12}$	100	1.7-4.7	261.70	50/189.80	[1]
α-$Na_{0.67}MnO_{2.26}$	250	2.0-4.3	110	40/105	[2]
$Na_{0.7}MnO_{2.05}$-$Na_{0.91}MnO_2$	200 1000	2.0-4.5	133.15 83.12	100/108.38 700/61.71	This work

(a)

Potentials	$R_1(\Omega)$	$R_2(\Omega)$
OCV	4.96	125.20
3.6 V	4.92	122.90
3.9 V	4.81	126.40
4.5 V (1st charge)	5.46	165.50
3.9 V	5.27	150.70
3.0 V	4.98	117.70
2.0 V (1st full discharge)	5.06	110.30
2.8 V	4.92	120.30
3.2 V	4.86	127.10
4.1 V	5.05	127.10
4.5 V	4.25	139.40
constant voltage charge 4.5 V (2nd full charge)	8.22	138.00
3.8 V	11.99	103.99
3.0 V	3.08	88.42
2.0 V (2nd full discharge)	3.55	115.90

(b)

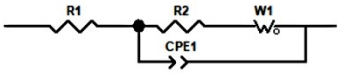

Fig. S5 (a) Impedance list of the charge-discharge cycle, (b) equivalent circuit.

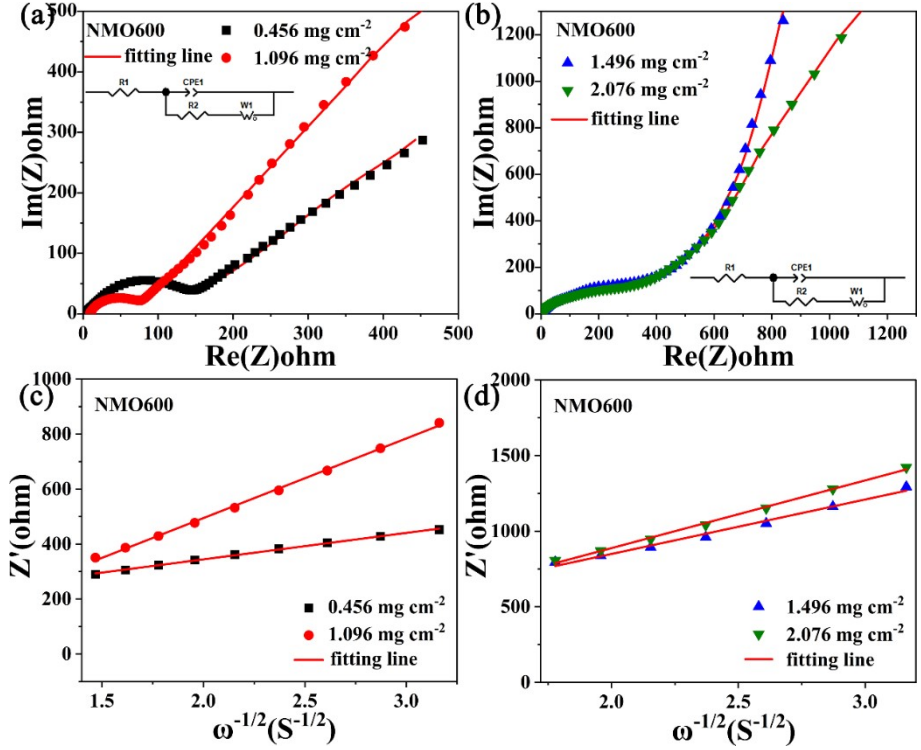

Fig. S6 The EIS of NMO600 (a-b) the AC impedance, (c-d) the equivalent circuit fitting curve.

Table S3 Data of each electrochemical component of as-prepared samples.

samples	R_1 (Ω)	R_2 (Ω)	D_{Li}^+ ($cm^2\ s^{-1}$)
NMO600(0.456 mg cm^{-2})	4.36	138.00	6.19×10^{-9}
NMO600(1.096 mg cm^{-2})	9.29	62.98	6.84×10^{-10}
NMO600(1.496 mg cm^{-2})	2.04	305.00	4.43×10^{-10}
NMO600(2.076 mg cm^{-2})	2.41	275.00	2.86×10^{-10}

R_1: solution impedance, R_2: charge transfer impedance.

In order to further explore the conductivity of prepared samples, the electrochemical impedance were tested, respectively, as shown in Fig. S3. The AC impedance diagram is mainly composed of three parts. The intersection of the semi-circle and the real axis in AC impedance is the total internal resistance (R_s). The fitting data are shown in Table 1. In the AC impedance test of lithium ion batteries, the resistance of NMO600 (0.456 mg cm^{-2}) (62.98 Ω) is smaller than that of NMO600 (1.096 mg cm^{-2}) (138.00 Ω), NMO600 (1.496 mg cm^{-2}) (305.00 Ω) and NMO600 (2.076 mg cm^{-2}) (275.00 Ω).

The dynamics of heterostructures cathodes were studied, the lithium diffusion coefficients (D_{Li}^+) were calculated through the equation (5) and equation (6)

$$Z=R_1+R_2+\delta_\omega^{-1/2} \quad (5)$$

$$D=R_2T^2/2n^4\delta^2C^2A^2F^4 \quad (6)$$

Where R is the gas constant (8.3145 J mol^{-1} K^{-1}), T is the thermodynamic temperature (298 K), C is the concentration of Li^+, n is the electron transfer number, A is the electrode surface area (0.785 cm^2), and F is the Faraday constant (96485 C mol^{-1}). As shown in Table S1, the D_{Li}^+ values for NMO600 (0.456 mg cm^{-2}), (1.096 mg cm^{-2}), (1.496 mg cm^{-2}), (2.076 mg cm^{-2}) were 6.19×10^{-9}, 6.84×10^{-10}, 4.43×10^{-10}, 2.86×10^{-10} $cm^2\ s^{-1}$.

References

1. X.-J. Gu, Y.J. Cai, X. Yao, H.-L. Tian and Z. Su, New J. Chem. 2022, 46, 21350.

2. S.-Y. Yang, X.-Y. Wang, W. Wu, T. Hu, X. Wang and S.-Y. Yi, Journal of Central South University. 2009, 40, 72-77.